Mon. Not. R. Astron. Soc. (1992) **259**, 569–575

In the vicinity of a rotating black hole: a fast numerical code for computing observational effects

V. Karas,[1,2] D. Vokrouhlický[1,3] and A. G. Polnarev[4,5]

[1] *Astronomical Institute, Charles University, Švédská 8, CS-150 00 Prague, Czechoslovakia*
[2] *NORDITA, Blegdamsvej 17, DK-2100 Copenhagen Ø, Denmark*
[3] *Observatoire de la Côte d'Azur, dept. CERGA, Av. Nicolas Copernic, F-06130 Grasse, France*
[4] *Astro-Space Centre, P. N. Lebedev Physical Institute, 84/32 Profsoyuznaya st., Moscow, 117810, Russia*
[5] *Institute of Astronomy, Madingley Road, Cambridge CB3 0HA*

Accepted 1992 June 1. Received 1992 April 24; in original form 1992 February 28

ABSTRACT

We describe a numerical code which has been developed to calculate images of various effects occurring in the close vicinity of a rotating (Kerr) black hole, as seen by a distant observer. Null geodesics are first integrated numerically, fitted by Chebyshev polynomials, and their shape stored in the computer. In this way, for a given set of parameters describing the configuration of the black hole and position of the observer, we obtain a 'catalogue' of photon paths which is then used by subsequent codes adapted to specific problems. Several astrophysically meaningful examples are given, in particular photometric light curves of a bright spot located on the surface of an accretion disc and orbiting the black hole.

This approach enables us to speed up appropriate application codes by approximately two orders of magnitude. In comparison with a direct scheme where application codes integrate many geodesics each time they are needed, our approach has advantages when a number of tasks (with, for example, different models of the spot shape and radiation) are computed for a given configuration of the black hole parameters and the observer's inclination angle.

Key words: accretion, accretion discs – black hole physics – radiative transfer – relativity – methods: numerical – galaxies: active.

1 INTRODUCTION

Active galactic nuclei (AGN) are generally believed to contain a compact object (presumably a supermassive black hole) in their cores. The black hole is surrounded by a plasma which forms an accretion disc. The angular momentum of the black hole is probably non-zero. One of the most promising approaches, the Blandford–Znajek scenario (1977), employs the model of a rotating black hole as a unified way of explaining the origin of energy release from various types of AGN. On the other hand, despite great effort over the last few decades, details of the configuration remain unclear. Therefore it is of great astrophysical interest to have an efficient tool for checking the observational consequences of various processes which may occur in the vicinity of a Kerr black hole. The gravitational field of a rotating black hole is described by the Kerr metric to high accuracy, because this is a unique metric corresponding to the vacuum, axisymmetric, stationary and asymptotically flat space–time (see for example Novikov & Frolov 1989 and references therein) – conditions which are approximately satisfied in the vicinity of an astrophysical black hole. The Kerr metric can also describe, to some extent, the gravitational fields of other compact objects like neutron stars (Butterworth & Ipser 1976; Komatsu, Eriguchi & Hachisu 1989). Our approach can thus be useful in visualizing the shapes of neutron stars, a problem that has been solved by several authors (e.g. Winterberg & Phillips 1973; Nollert et al. 1989; Bičák & Ledvinka, in preparation). Extensive integrations of photon paths in a curved geometry have been performed by, e.g., Cunningham & Bardeen (1973), Cunningham (1975, 1976), Luminet (1979), Polnarev & Turchaninov (1979), Sikora (1979), Fukue & Yokoyama (1988) and Zakharov & Polnarev (1988) to obtain the appearance of a star orbiting round a rotating black hole or of an accretion disc near the black hole.

The main aim of this paper is to introduce a series of codes which are flexible enough to deal with various

problems after minor modifications (specification of the accretion disc model, for example). In the next section we give a detailed description of our approach. We try not to go into detail of particular problems in this paper. Nevertheless, in Section 3 we demonstrate several applications, illustrating how our code could be used in connection with some current investigations in the field. For example, we discuss light curves of a bright spot orbiting the black hole on an orbit close to the black hole horizon, taking into account different positions and lifetimes of the spot, evolution of its shape and intrinsic luminosity, and the simultaneous contribution of a large number of spots.

2 DETAILS OF THE NUMERICAL APPROACH

2.1 Basic equations

We calculate observable effects in the reference frame of a distant observer who is at rest with respect to Boyer–Lindquist coordinates (e.g. Misner, Thorne & Wheeler 1973) $(r=r_o,\ \theta=\theta_o,\ \phi=0,\ t)$. We use a geometrized radial coordinate r in units of the mass of the black hole M [$M\approx 10^{13}\,M_8$ (cm) where M_8 is mass in units of 10^8 $M_\odot$]; r is thus a dimensionless quantity. For the gravitational radius in these units we obtain $r_+\equiv[1+(1-a^{*2})^{1/2}]$, where $a^*=a/M$ is the angular momentum parameter of the black hole. The equation of a null geodesic can be written in integral form (Carter 1968):

$$\int_{r_o}^{r} R(r')^{-1/2}\,\mathrm{d}r' = \int_{\theta_o}^{\theta} \Theta(\theta')^{-1/2}\,\mathrm{d}\theta' = \int_{\phi_o}^{\phi} F(\phi')^{-1}\,\mathrm{d}\phi',$$

$$t = \int_{t_o}^{t} \frac{A-2a^*r\xi}{\Sigma\Delta}\,\mathrm{d}\tau, \qquad (2.1)$$

with

$$R(r)=r^4+(a^{*2}-\xi^2-\eta)r^2+2[\eta+(\xi-a^*)^2]r-a^{*2}\eta,$$

$$\Theta(\theta)=\eta+a^{*2}\cos^2\theta-\xi^2\cot^2\theta,$$

$$F(\phi)=[2a^*r+(\Sigma-2r)\xi\csc^2\theta]\Delta^{-1}, \qquad (2.2)$$

and

$$\Delta=r^2-2r+a^{*2}, \qquad \Sigma=r^2+a^{*2}\cos^2\theta,$$

$$A=(r^2+a^{*2})^2-\Delta a^{*2}\sin^2\theta.$$

In (2.1) τ is an affine parameter along the photon trajectory. The particular photon path is completely described by initial conditions and two constants of the motion, ξ and η. In general, for a locally non-rotating observer, we can associate ξ and η with angles α and β on his local sky (Page & Thorne 1974; Polnarev & Turchaninov 1979) $(0\le\alpha\le\pi,\ 0\le\beta<2\pi$; Fig. 1a) by the relations

$$\xi=\left(\frac{A^{1/2}\sin\theta\sin\alpha\sin\beta}{\Sigma^{1/2}\epsilon}\right)_{\tau_o,\theta_o},$$

$$\eta=\frac{1}{\Delta}(r^2+a^{*2}-a^*\xi)^2-\Sigma\epsilon^{-2}\cos^2\alpha-\xi^2+2a^*\xi-a^{*2}\Big|_{r_o,\theta_o} \qquad (2.3)$$

where

$$\epsilon=(\Sigma^{1/2}\Delta^{1/2}+2a^*r\Sigma^{-1/2}\sin\theta\sin\alpha\sin\beta)A^{-1/2}. \qquad (2.4)$$

In our applications, however, the observer is located far from the black hole, $r_o\to\infty$, and we are interested in null lines which asymptotically follow the straight lines going at the inclination angle θ_o. We thus introduce two polar coordinates in the plane perpendicular to the direction θ_o, the impact parameter ρ and azimuth ψ (Fig. 1b), by the relations

$$\sin\theta\sin\alpha\cos\beta=\cos\theta_o-\cos\alpha\cos\theta,$$

$$r\cos\theta=r_o\cos\theta_o-\rho\sin\theta_o\cos\psi,$$

$$r\cos\alpha=r_o, \qquad (2.5)$$

with $r=(r_o^2+\rho^2)^{1/2}$.

2.2 Description of the code

First we describe how the 'catalogue' of null geodesics is generated. Each catalogue is characterized by two parameters: the angular momentum parameter of the black hole, a^*, and inclination angle of the observer, θ_o. Each curve in the catalogue is characterized by initial values $\rho=\rho_0$, $\psi=\psi_0$. We find it useful for the applications under consideration to

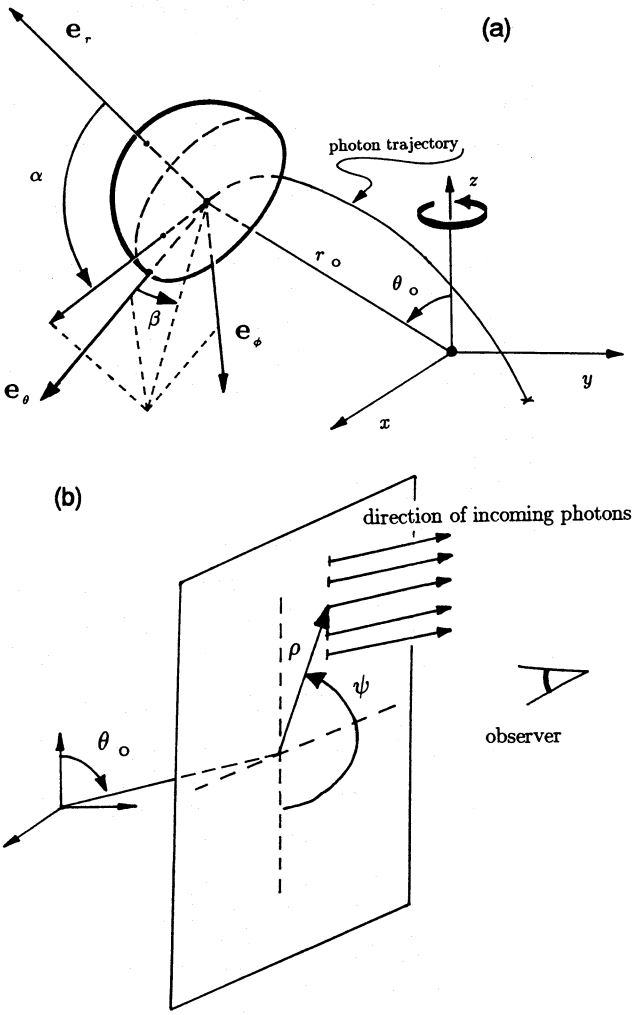

Figure 1. Coordinates used in this paper.

choose the range in impact parameter to be $\rho \lesssim 200\, r_+$, with appropriate steps in ρ and ψ which give a finer grid for geodesics that eventually enter the region close to the black hole. One catalogue contains data for about 10^4 geodesics. The curves are integrated (using the step-adaptive 4–5 Runge–Kutta method) until they cross the equatorial plane. In practice, equations (2.1)–(2.4) in their exact form are used only below some radial distance ($500\, r_+$, say); outside this region the shape of the geodesics is approximated by straight lines in a nearly flat space–time. After crossing the equatorial plane, the curve is followed in the opposite direction to check the accuracy of the integration routine. The curve is then fitted with a Chebyshev polynomial. (It is a well-known result of the theory of fitting numerical data that this form of the fit minimizes, roughly speaking, the maximum deviation of the approximation with a minimum order of the polynomial; see, e.g., Press et al. 1986.) The fit has a parametric form: $x(\tau)$, $y(\tau)$, $z(\tau)$ and $t(\tau)$ where $\{x, y, z\}$ are related to $\{r, \theta, \phi\}$ like spherical coordinates, by definition. [The relationship between Boyer–Lindquist's $\{r, \theta, \phi, t\}$ and the $\{x, y, z, t\}$ which are actually fitted is of course not unambiguous. This simplest choice has an obvious advantage: far from the hole the trajectories are nearly straight and they can be fitted with a low-order polynomial.] The form of the trajectories becomes complicated and differs substantially from straight lines only very close to the horizon. It is also possible to use Kerr ingoing coordinates, which may have some advantages in comparison with Boyer–Lindquist coordinates in describing frame-dragging effects on photon trajectories; however, the shape of a *general* null geodesic near the horizon is not much simpler in these coordinates. The actual order of the polynomial (50 at maximum) is established according to the prescribed accuracy of the approximation (typically ± 0.02 in dimensionless units defined above). Some curves in the close vicinity of the horizon have rather complicated shapes and need to be split into two parts, each of which is fitted separately.

In other words, integration of the curves in the catalogue starts at the location of the observer and proceeds *towards* the black hole. As we shall be mostly interested in light signals coming *from* central regions of an accretion disc toward the distant observer, we actually deal with the curves in the opposite direction. We take into account that the equations of null geodesics are invariant under the substitution $\xi \to -\xi$, $a^* \to -a^*$ and $\tau \to -\tau$ with simultaneous change of the bounds of the last integral in (2.1), $\phi \leftrightarrow \phi_o$ (see equations 2.1–2.4). This means that the shape of the light rays will be the same as is stored in the catalogue, if we interpret the curves in the coordinate system with oppositely oriented azimuthal coordinate and $\{x, y, z\} \to \{x, -y, z\}$ and we restore a^* and ξ to their original values.

Coefficients of the Chebyshev polynomials are stored in the form of direct access files. Data on any curve in the catalogue are, therefore, directly accessible, which is important for our applications. It should be emphasized that there is enough information to restore not only the shape of the curve in space but also the light traveltime and the effects of time delay. To speed up the application program, one can extract only the part of the catalogue which is immediately relevant (for example, when only the innermost regions are to be investigated), or one can merge two catalogues (when a large disc is to be studied).

Fig. 2 represents points of intersection of photon trajectories included in our catalogue with the equatorial plane. These points of intersection are marked by small circles. Shown also is the finer grid (marked by the points) which has

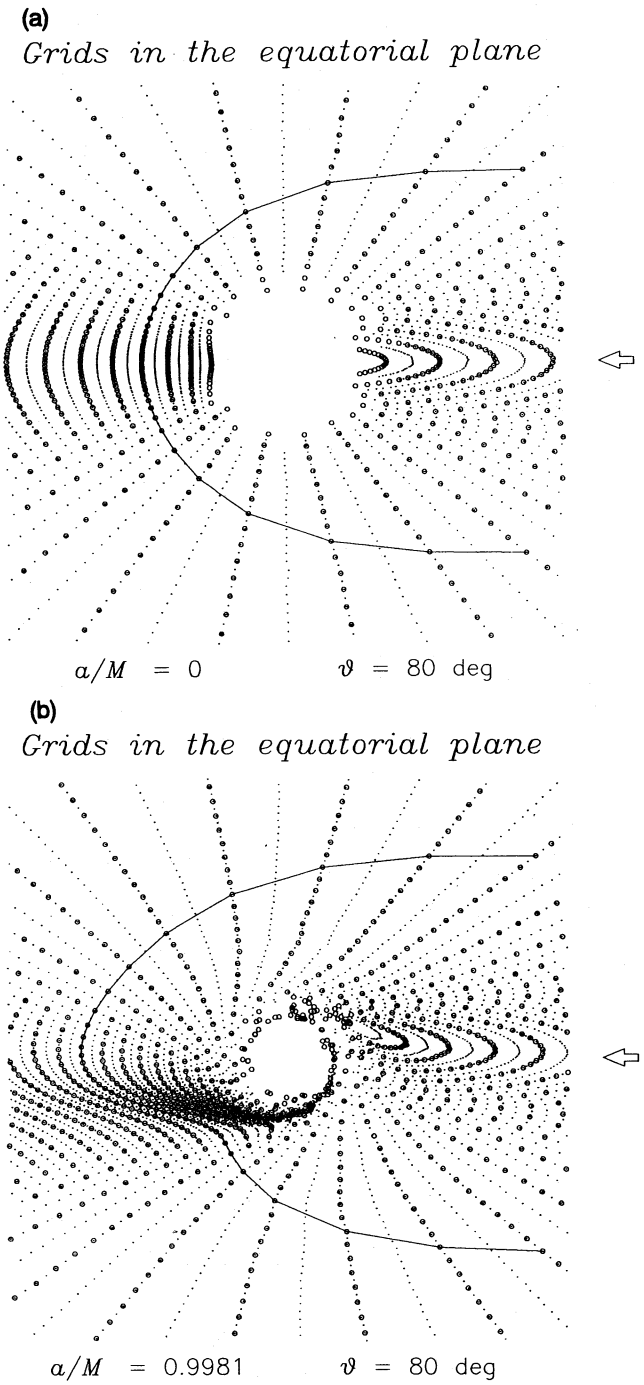

Figure 2. Intersections of null geodesics from the catalogue with the equatorial plane in the region close to the black hole (up to $r \approx 6$) are marked by small circles. Points denote the finer grid of intersections of the curves which are obtained from the catalogue by approximations using the geodesic deviation equation. Values of the angular momentum parameter $a^* = a/M$ and the inclination of the observer θ_o are given for each figure. The arrow denotes the location of the observer. The solid curve is a projection of the circle ρ = constant in the observer's frame on to the equatorial plane. Note the deformation of the curve when the black hole rotates.

been generated with the help of the catalogue. Each curve corresponding to a point of this finer grid is constructed by interpolation using three neighbouring curves of the catalogue. In other words, in looking for a photon ray with some specified initial conditions, we look for three geodesics with nearby initial conditions and then, by linear approximation which is very similar to the method of geodesic deviation, we find the initially specified curve. (The grid of the reference catalogue should be certainly fine enough.) Operating in this way, the application program, suited to some particular problem which uses the catalogue, can effectively create *as fine a grid as is required* by the problem under consideration.

Analogously, Fig. 3 shows the intersections of the grid with a thick disc. We have chosen typical disc height profiles which one meets in models of thick discs. Some parts of the thick disc are self-eclipsed; the innermost visible region is, on the other hand, larger when bending of light rays is taken into account (cf. Karas & Bao 1992). It is a trivial but geometrically rather complicated task to find these intersections, even in a flat space–time, when thick discs of general shape are considered.

2.3 Estimation of the speed

The efficiency of the code depends on the character of the problem which is to be solved. For example, our scheme appears especially convenient for studying the effects connected with finite-sized bright spots located on the disc surface (see Section 3), possibly with a complicated shape and structure. In this way, our code is complementary to the work of, e.g., Bao (1992) and others, who have studied mainly point-like sources. The main advantage of our approach comes when the application codes use the catalogue many times and when large numbers of geodesics are integrated repeatedly. This is the case of computing observed radiation from different disc models which can be non-stationary or contain evolving inhomogeneities (like orbiting bright spots). Naturally, our method cannot be efficient if one computes only one kind of problem, so that the CPU time required to create the catalogue is comparable to that required to solve the problem directly.

The code has been written in FORTRAN 77 and run on an IBM 3090 computer. Intersections of geodesics with the equatorial plane can be found approximately two orders of magnitude faster than by direct integration. The efficiency is only slightly lower with a thick disc, when self-eclipses occur.

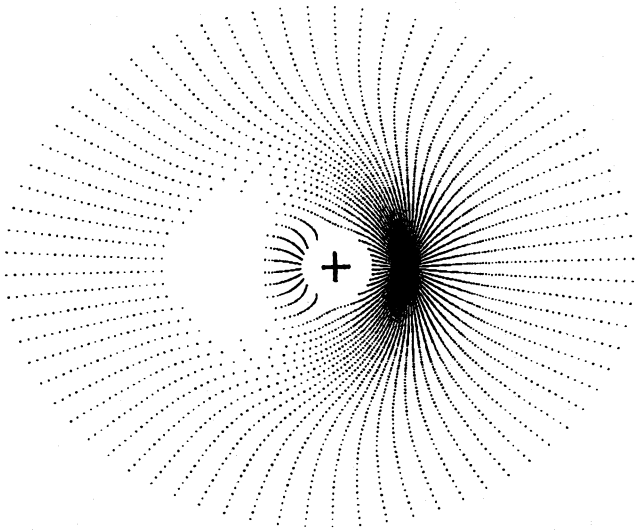

Figure 3. As Fig. 2 but for a thick disc. Intersections of photon paths with the disc surface are shown. The black hole is marked by a cross in the centre of the disc. The region $r < 200$ is shown.

3 EXAMPLES

Now, without going into detail and discussion of any special models, we give a few examples where the adoption of our approach may be useful.

The photometric light curve of a bright object orbiting a black hole was discussed in a classical paper by Cunningham & Bardeen (1973). Astrophysical applications have been considered by Asaoka (1989) and Bao (1992). Abramowicz et al. (1992) suggested that periodic peaks in the light curve of NGC 6814 may be due to the circular motion of a bright spot, and Abramowicz (1992) discussed possible configurations of the system in greater detail. Models with a large number of spots have been discussed recently (Abramowicz et al. 1991), and they appear relevant for the proper modelling of AGN short-term variability. Spots with different sizes, lifetimes, anisotropic radiation, etc. must be considered. These characteristics affect the light curves and they probably have not been discussed in the literature.

Figs 4–6 show light curves of a single finite-sized spot. The intrinsic luminosity of the spot decreases exponentially with distance from the centre of the spot (with characteristic radius $\delta r = 0.5$) and is time-independent. The figures are drawn in dimensionless units; the flux F is obtained by integrating the intensity over the observer's local sky and normalizing to its maximum value. Time is measured in revolutions around the central object: $time = 2\pi(r^{3/2} + a^*)$, where r is the radial distance of the spot. In conventional units, time is rewritten in the following way:

$$t \approx 8.2 \frac{M}{10^8\ \mathrm{M}_\odot}\ time\,(\mathrm{min}). \tag{3.1}$$

For large θ_o, the main peak occurs when the spot is behind the black hole ($time \approx 0.5$; exactly 0.5 in the Schwarzschild case) and is a result of the focusing effect. The secondary peak occurs approximately at $time = 0.75$ and is caused by the Doppler effect. The Doppler effect becomes important for smaller inclination angles; the light curves in this case are nearly symmetric with respect to $time = 0.75$. However, for a given inclination, the relative importance of the Doppler effect with respect to the focusing effect decreases with decreasing radial distance of the spot from the black hole. It is easily seen, for the case in which the inclination is 80° and the radial position of the spot $r \lesssim 6$, that the focusing effect dominates the curve while the contribution from the Doppler effect is negligible in comparison; for this reason the curve becomes nearly symmetrical again, but now with respect to $time = 0.5$. An analogous effect would naturally occur in the case of a non-rotating Schwarzschild black hole ($a^* = 0$), but in the case of a rapidly rotating black hole ($a^* \to 1$) this effect can be considerably more prominent because stable orbits of matter extend closer to the black hole horizon.

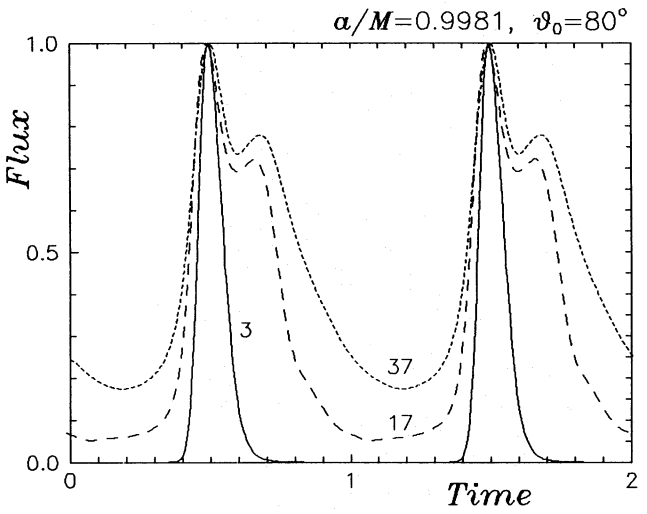

Figure 4. Typical profiles of the light curves in dimensionless units. The radial position of the centre of the spot is given with each curve.

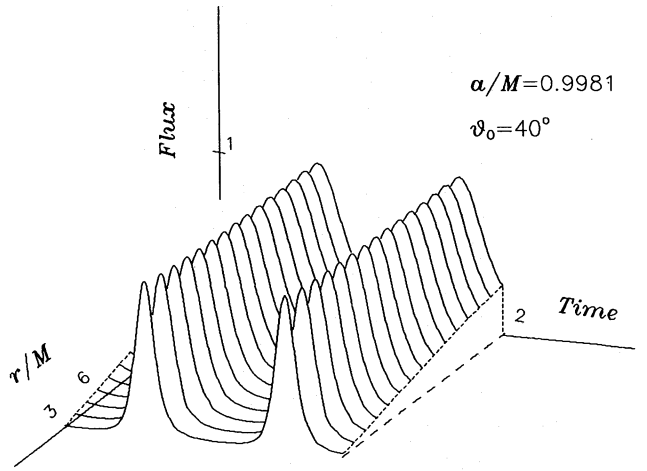

Figure 5. Light curves corresponding to various positions of the spot in the range $3r_+ < r < 17r_+$. For small inclinations, each curve has only one peak due to the Doppler effect. The flux is normalized to its maximum value. The absolute value of $F_{r=3r_+}/F_{r=17r_+} = 0.55$.

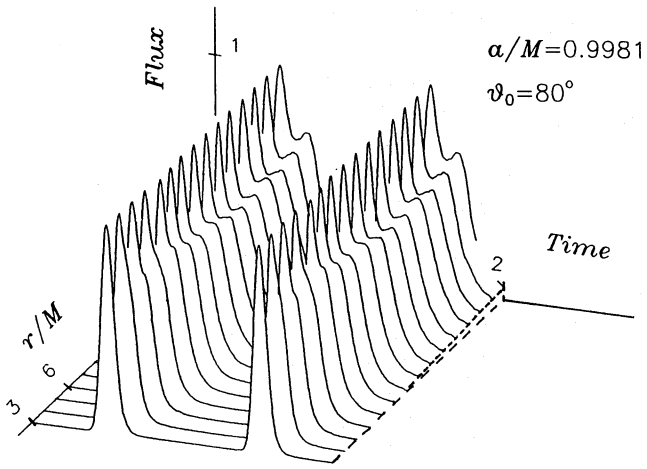

Figure 6. As Fig. 5 but for a larger inclination (more edge-on). Now the peaks due to the focusing effect dominate, and for the absolute value of the flux we have $F_{r=3r_+}/F_{r=17r_+} = 4.4$. Note that this ratio depends strongly on the mutual interplay between the gravitational redshift, Doppler effect and focusing effect, and thus on the inclination angle, which may have important observational consequences.

Fig. 7 shows the light curve due to a single spot as in the previous figures, but now the shape and intrinsic luminosity of the spot evolve with time. Initially the spot has a circular shape. Each point element of matter in the spot revolves with a Keplerian velocity corresponding to the radial position of this element. Since, after several revolutions, the size of the spot in the azimuthal direction is much larger than in the radial direction, both Doppler and focusing effects integrated over the spot become too small to affect the light curve.

Fig. 8 shows a weak dependence of the location of peaks in the light curve on the radial position of the spot and the inclination angle. This dependence is a result of gravitational lensing (deflection of light) and the time-delay effect.

Fig. 9 illustrates that for smaller spots the profile of the light curve gets narrower than for spots of larger size. This is expected because the operation of both Doppler and focusing effects is sharper when the spot becomes point-like. The intensity integrated over frequency in the locally comoving frame corotating with the spot is taken to be $I \propto T_{\rm eff}^4$ with $T_{\rm eff} \propto \exp(-\sigma\delta r^2)$, where δr is the local distance from the spot centre and σ is a constant. Thus for $\sigma = 1$, for example, the intensity decreases to 1/e of its value in the centre of the spot at a distance $\delta r = 0.5$. Fig. 9 illustrates the dependence of the FWHM of the light-curve profile on spot size.

Fig. 10 shows the light curve produced by 10 spots located in the region $3r_+ \le r \le 17r_+$. Two inclination angles are considered in Figs 10(a) and (b), respectively. Intrinsic luminosities of the spots are assumed to decrease exponentially with time. Initial values for these luminosities, e-folding times for their decay, and initial locations of the spots have been chosen as random variables in some range, given by a random number generator which started with identical sequences of numbers for both cases (a) and (b). Thus the difference between these two figures is due to different inclination angles only. Fig. 11 shows the light curve as in Fig. 10, but for a total number of spots equal to 100. It

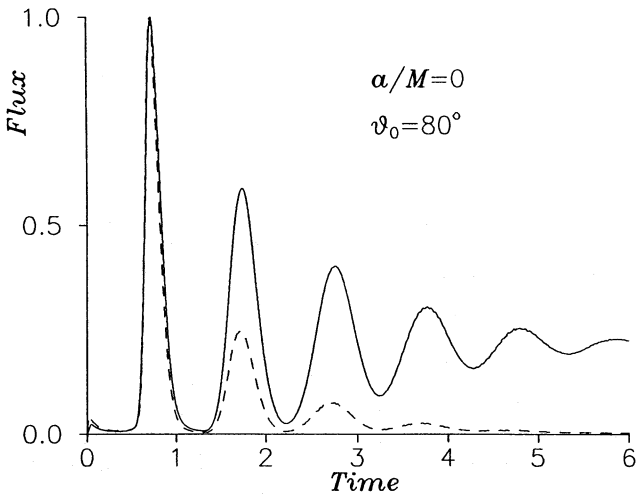

Figure 7. Light curve of finite-sized spot (characteristic radius 0.5 M) which rotates differentially at $r = 6r_+$ and becomes very elongated after several revolutions. The solid curve corresponds to a spot with constant intrinsic luminosity, while the dashed curve corresponds to a spot the intrinsic luminosity of which decreases exponentially with time (the e-folding time is 5 revolutions).

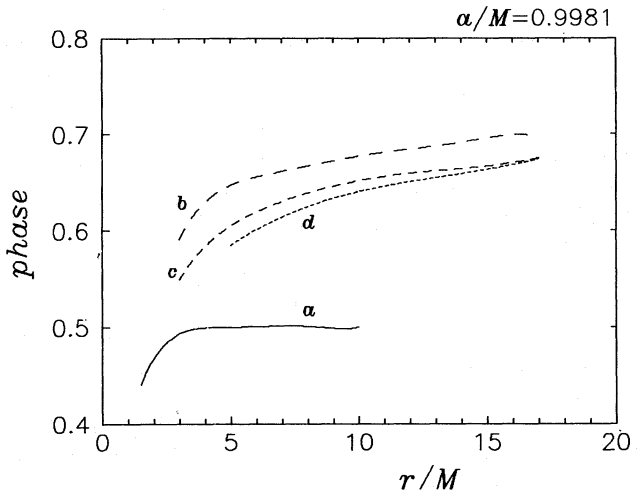

Figure 8. Position of the peak in the light curve. For a spot which is located far from the black hole, the focusing effect is a maximum at phase ≈ 0.5 (when the spot is behind the black hole) and the Doppler effect is a maximum at ≈ 0.75 (when the spot approaches the observer). Curve (a) corresponds to the peak due to focusing and (d) to the peak due to the Doppler effect when $\theta_0 = 80°$ (cf. Fig. 6). For inclinations of 40° (b; cf. Fig. 5) and 60° (c) there is no focusing effect and the only peak is due to the Doppler effect. When the spot is far from the black hole ($r/M \approx 15$ in this figure), the importance of light bending decreases; the phase of the focusing peak approaches 0.5 and that of the Doppler peak goes to ≈ 0.7. The difference from 0.75 is then caused solely by the time-delay effect.

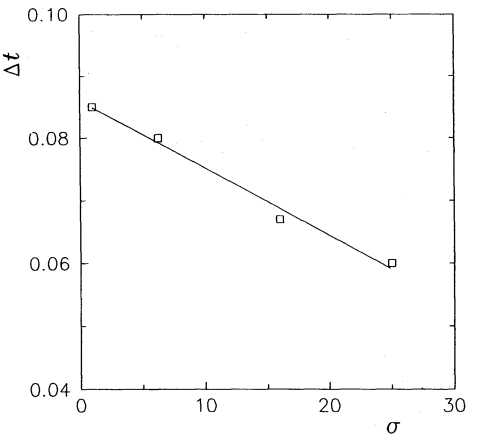

Figure 9. FWHM of the light-curve profile as a function of its characteristic radius which is equal to $\sigma^{-1/2}$; large σ thus corresponds to smaller spot-size.

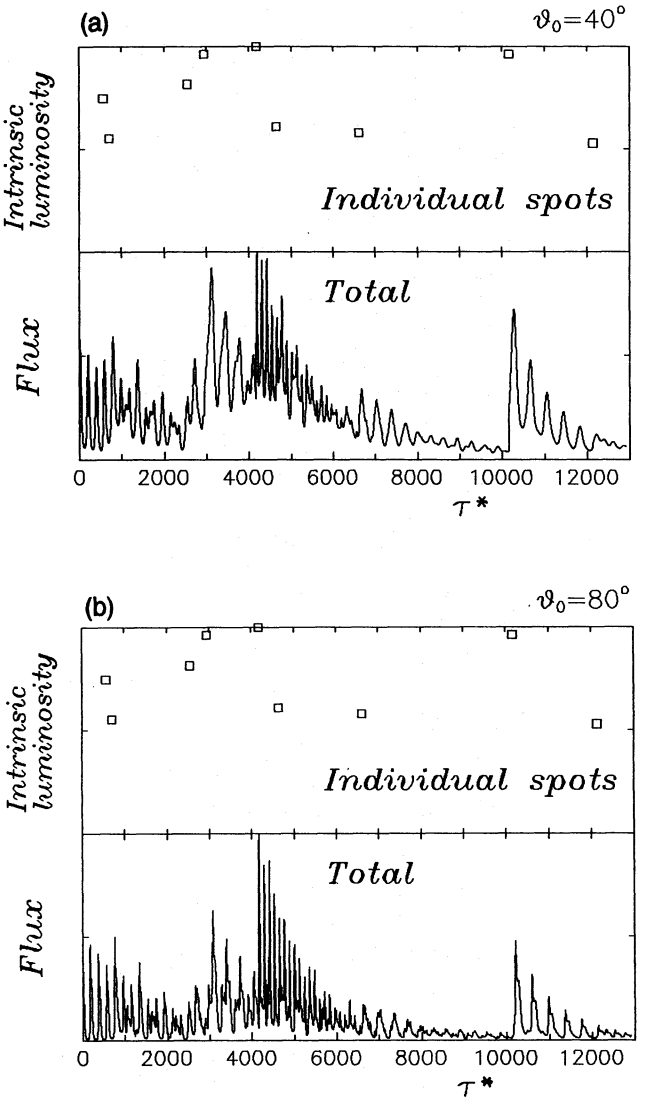

Figure 10. (a) Superposition of the light curves due to 10 orbiting spots with different intrinsic characteristics. The initial local luminosity of selected spots (normalized to the maximum value) is given in the upper part of the figure. The lower part shows the resulting simulated light curve. Alternatively, one could normalize the flux to its average value. Then larger inclination would correspond to larger variability of the source, because in that case the focusing strongly affects the light of spots orbiting very close to the black hole (we assume an isotropic distribution of the luminosity of individual spots in their local frame). (b) As (a) but for $\theta_0 = 80°$.

has been suggested by Abramowicz et al. (1991) that the short-term X-ray variability of AGN may be due to a large number of spots located on the accretion disc. In both these figures, time τ^* is plotted in units of the orbital period of the outermost spot [equation (3.1) with $r = 17 r_+$].

The code can also be used to compute spectra of accretion discs, provided that their half-thicknesses, local luminosities, distributions of radiation intensity in the local frame, orbital velocities, etc. are given. The shapes of the spectra are much more θ_0-dependent when non-relativistic self-eclipses due to finite thickness are taken into account (Madau 1988). Spectra of relativistic discs have been studied by a number of authors in various approximations (e.g. Cunningham 1975, 1976; Laor & Netzer 1989; Asaoka 1989). In particular, the current interest in intensities and profiles of the iron Kα line emitted from an accretion disc requires the repetition of the calculations under various conditions (Fabian et al. 1989; Laor 1991; Matt et al. 1992). The combination of geometrical (i.e. due to finite thickness) and relativistic self-eclipses, treated separately in numerous works, might result in consequences which would turn out to be very important for the comparison of previous disc models with observations.

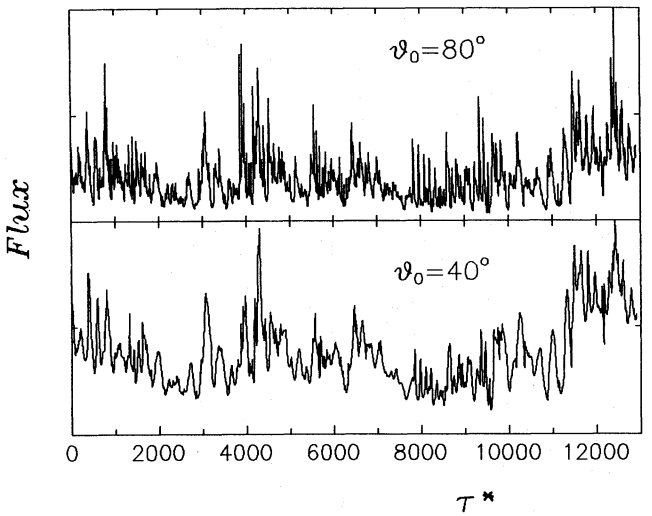

Figure 11. The light curve, as in Fig. 10, but for 100 randomly generated spots.

ACKNOWLEDGMENTS

We thank M. A. Abramowicz for helpful discussions, Y. Eriguchi for several suggestions which helped us to improve our manuscript, and B. Pagel for a careful reading of the paper. Our thanks are also due to J. Bičák, A. Lanza and O. Semerák for useful comments at the early stages of this work. This research was partially supported by the IBM Academic Initiative in Czechoslovakia. VK acknowledges financial support and kind hospitality from NORDITA. AP acknowledges NORDITA, SISSA (Trieste, Italy) and the Institute of Astronomy (Cambridge, UK) for hospitality.

REFERENCES

Abramowicz M. A., 1992, in Proc. 2nd Maryland Astrophysical Conference. New York Acad. Sci. Press, New York
Abramowicz M. A., Bao G., Lanza A., Zhang X.-H., 1991, A&A, 245, 454
Abramowicz M. A., Lanza A., Spiegel E. A., Szuszkiewicz E., 1992, Nat, 356, 41
Asaoka I., 1989, PASJ, 41, 763
Bao G., 1992, A&A, 257, 594
Blandford R. D., Znajek R. L., 1977, MNRAS, 179, 433
Butterworth E. M., Ipser J. R., 1976, ApJ, 204, 200
Carter B., 1968, Phys. Rev., 174, 1559
Cunningham C. T., 1975, ApJ, 202, 788
Cunningham C. T., 1976, ApJ, 208, 534
Cunningham C. T., Bardeen J. M., 1973, ApJ, 183, 237
Fabian A. C., Rees M. J., Stella L., White N. E., 1989, MNRAS, 238, 729
Fukue J., Yokoyama T., 1988, PASJ, 40, 15
Karas V., Bao G., 1992, A&A, 257, 531
Komatsu H., Eriguchi Y., Hachisu I., 1989, MNRAS, 239, 153
Laor A., 1991, ApJ, 376, 90
Laor A., Netzer H., 1989, MNRAS, 238, 897
Luminet J.-P., 1979, A&A, 75, 228
Madau P., 1988, ApJ, 327, 116
Matt G., Perola G. C., Piro L., Stella L., 1992, A&A, 257, 63
Misner C. W., Thorne K. S., Wheeler J. A., 1973, Gravitation. Freeman, San Francisco
Nollert H. P., Kraus U., Rebetzky A., Herold H., Maile T., Ruder H., 1989, in Hunt J., Battrick B., eds, 23rd ESLAB Symp. Two Topics in X-ray Astronomy. Vol. 1, ESA, Paris, p. 551
Novikov I. D., Frolov V. P., 1989, Physics of Black Holes. Kluwer, Dordrecht
Page D. N., Thorne K. S., 1974, ApJ, 191, 499
Polnarev A. G., Turchaninov V. I., 1979, Acta Astron., 29, 81
Press W. H., Flannery B. P., Teukolsky S. A., Vetterling W. T., 1986, Numerical Recipes. Cambridge Univ. Press, Cambridge
Sikora M., 1979, Acta Astron., 29, 87
Winterberg F., Phillips W. G., 1973, Phys. Rev. D, 8, 3329
Zakharov A. P., Polnarev A. G., 1988, preprint (in Russian)